JMEMS Letters

A Hybrid Flapping-Blade Wind Energy Harvester Based on Vortex Shedding Effect

Tao Chen, Yuedong Xia, Wenjie Liu, Huicong Liu, Lining Sun, and Chengkuo Lee

***Abstract*— We proposed a hybrid piezoelectric and triboelectric-based wind energy harvester with high output performance. A square-shaped flapping blade and two spindle-shaped outer frames are specifically designed to enhance the vortex shedding effect. As wind flows across the device, both the piezoelectric and triboelectric parts produce power outputs at the same time. The cut-in wind speed of the device is as low as 4 m/s and the voltage outputs get improved with the increase in wind speed. As wind speed reaches 14 m/s, the open circuit peak voltage outputs of the piezoelectric, and the upper triboelectric parts are 19.8 and 17.4 V, respectively. The maximum power outputs of these two parts can be obtained as 112 and 76 μW at a wind speed of 10 m/s, with optimized load resistances of 0.6 and 0.9 MΩ, respectively. [2016-0015]**

***Index Terms*— Wind energy harvesting, vortex shedding, hybrid, piezoelectric, triboelectric.**

I. Introduction

Over the past couple of years, there has been growing interest dedicated to develop various energy harvesting devices. Ambient natural energy sources have been utilized, such as sunlight [1], sea wave [2], wind flow [3], temperature differences [4], and even human motions [5]. Wind energy is a clean, abundant and renewable source of energy. The conversion of wind flow into electricity can be realized by various physical mechanisms, for example, windmill structures, resonant cavity structures, or cantilever structures.

Windmill structures [6], [7] are widely adopted in wind energy harvesting design by using electromagnetic, piezoelectric and triboelectric mechanisms. They normally have outstanding power output, but the shortcomings are complicated structures and large volumes. Resonant cavity structures are commonly designed based on Helmholtz resonance. Sun *et al.* [8] proposed a piezoelectric WEH with a resonant cavity. AC voltage can be produced from the deformation of piezoelectric belt. Wang's group [9], [10] also demonstrated several similar prototypes using triboelectric mechanism. To achieve Helmholtz resonance, these devices normally have specific requirements for the structure size and wind speed, which limits their applications. Cantilever-type structure [11], [12] has a simple device configuration as compared with the other two. The working principle is based on wind-induced fluttering or vortex shedding effect. Electrical energy can be produced from the dynamic deformation of piezoelectric materials under the action of wind. There are also some electromagnetic WEHs [13] designed with cantilever structures. Electrical voltage can be generated from relative motion between magnet and coil. Cantilever-type WEHs [14], [15] can be easily fabricated, but the power output is not very satisfactory. Cantilevers like [11] and [12] have high resonant frequencies, but the vibration amplitudes are relatively small.

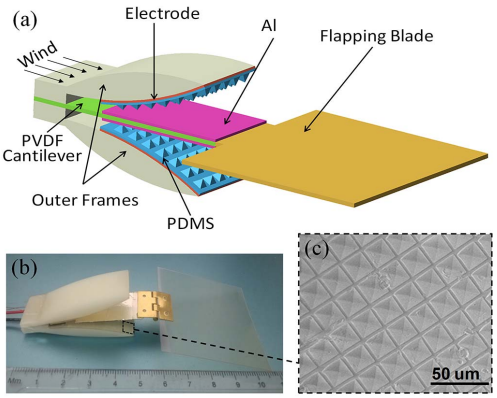

Fig. 1. (a) Schematic illustration of the hybrid WEH device. (b) Photograph of the proposed hybrid WEH device. (c) SEM photograph of the fabricated PDMS with pyramid structure.

In this letter, we proposed a hybrid flapping-blade WEH based on a flexible cantilever. Both the piezoelectric and triboelectric parts can generate power outputs from wind flow. The specific designs of flapping blade and outer frames can amplify the vibration of PVDF cantilever and the triboelectric contact. The output performance of the device will be enhanced dramatically at a relatively small volume and low wind speed.

II. Design and Characterization

Fig. 1(a) shows a schematic illustration of the hybrid WEH device, which consists of a flapping blade, a polyvinylidene fluoride (PVDF) cantilever, outer frames, friction films of aluminum (Al) and polydimethylsiloxane (PDMS). For piezoelectric part, a flexible PVDF cantilever is fixed at its tail end between two outer frames while the free end is connected with a flapping blade by a hinge. The dimensions of the PVDF cantilever are $52 \times 16 \times 0.2$ mm^3. For triboelectric part, Al foils with a thickness of 20 μm are attached on both sides of the PVDF cantilever to form a sandwich structure. The Al foils serve as friction surface as well as bottom electrode. Top electrode layers and PDMS films patterned with pyramid microstructures are attached on the inner arc surface of the upper and lower outer frames. Al foils and PDMS films are distributed face to face with the minimum and maximum spaces of 2 and 10 mm, respectively. The outer frame is specially designed as a spindle-shaped structure. The outer arc surface

Manuscript received February 3, 2016; revised May 28, 2016; accepted July 1, 2016. Date of publication July 21, 2016; date of current version September 29, 2016. This work was supported in part by the Foundation Research Project of Jiangsu Province under Grant BK 20140335, in part by the National Natural Science Foundation of China under Grant 51405318, and in part by the National High Technology Research and Development Program of China (863 Program) under Grant 2015AA043502. Subject Editor S. M. Spearing.

T. Chen, Y. Xia, W. Liu, H. Liu, and L. Sun are with the Jiangsu Provincial Key Laboratory of Advanced Robotics, Collaborative Innovation Center of Suzhou Nano Science and Technology, School of Mechanical and Electric Engineering, Soochow University, Suzhou 215123, China (e-mail: chent@suda.edu.cn; 20145229024@suda.edu.cn; liuwenjie@suda.edu.cn; hcliu078@suda.edu.cn; insun@hit.edu.cn).

C. Lee is with the Department of Electrical and Computer Engineering, National University of Singapore, Singapore 117576 (e-mail: elelc@nus.edu.sg).

Color versions of one or more of the figures in this letter are available online at http://ieeexplore.ieee.org.

Digital Object Identifier 10.1109/JMEMS.2016.2588529

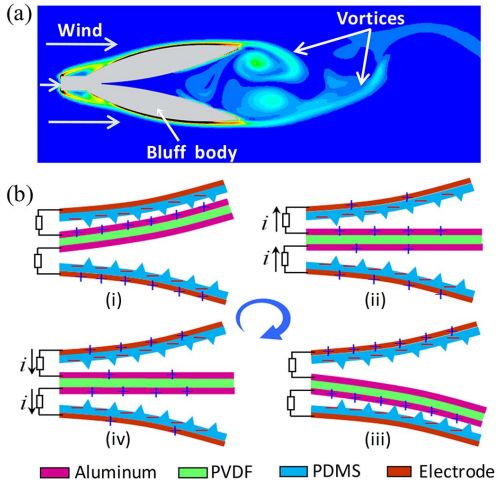

Fig. 2. (a) FEM simulation of the vorticity contours at wind speed of 5 m/s. (b) Illustration of the charge transfer process of triboelectric part.

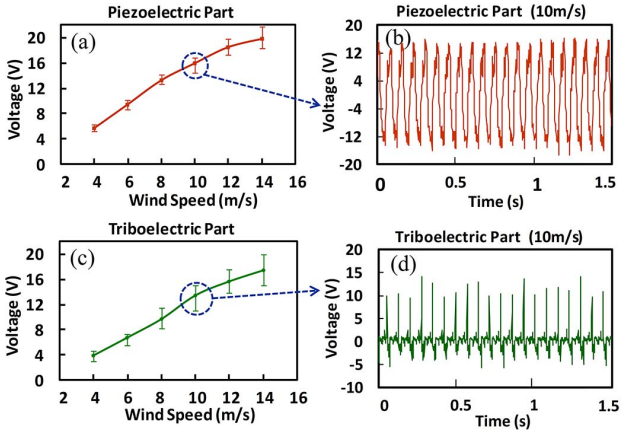

Fig. 3. Peak voltages of the piezoelectric (a) and upper triboelectric (c) parts at wind speed from 2 to 14 m/s. Voltage waveforms of these two parts (b) (d) at wind speed of 10 m/s.

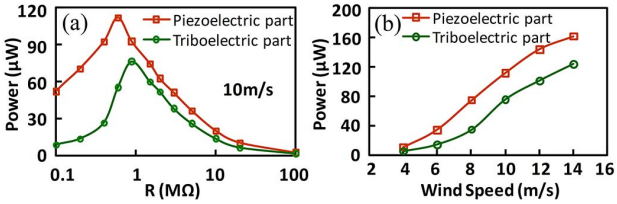

Fig. 4. Power characteristic of the piezoelectric and upper triboelectric parts at different load resistances (a) and wind speeds (b).

of the frame ensures the smooth flow of wind and the inner arc surface makes the two friction materials fully contact. Fig. 1(b) shows the photograph of the fabricated device. To enlarge the contact surface, the PDMS film with microstructures is prepared by using a silicon dioxide pyramid mold [16], [17]. The enlarged PDMS microstructure is shown in Fig. 1(c). The critical feature length of pyramid is 18 μm and the thickness of PDMS film is 160 μm. Flapping blade made of polyethylene terephthalate (PET) material is used to amplify the vibration of PVDF cantilever and increase the contact force of Al-PDMS, such that the output performance of the WEH device can be improved. The length of flapping blade is optimized as 50 mm.

The working principle of the hybrid WEH device is based on vortex shedding effect. When a wind flows past a bluff body, vortices will be created on both sides behind the bluff body in opposite rotation directions. For the WEH device, the outer frames serve as the bluff body and the vortices take place above and below the flapping blade. Fig. 2(a) shows the simulated vorticity contours of vortex street after bluff body. Due to the pressure differentials, the vortices can exert an alternating pressure force to the flapping blade in a direction transverse to the flow. Therefore, the flapping blade will oscillate upward and downward as wind flows through the device. Accordingly, the PVDF cantilever driven by the flapping blade deforms and contacts with the upper and lower inner surfaces of the outer frames. Piezoelectric-based voltage output can be generated in d_{31} mode. Meanwhile, the triboelectric-based voltage output based on a conjunction of triboelectrification effect and electrostatic induction occurs between the friction materials [18], [19].

Fig. 2(b) shows the process of charge transfer of the triboelectric part. There are two pairs of friction materials distributed on the upper and lower sides of the PVDF cantilever symmetrically. For the upper triboelectric part, the Al foils will get in contact with the PDMS film when the PVDF cantilever deforms closely to the upper outer frame as shown in Fig. 2(i). Negative charges on the Al foils are injected to PDMS film since PDMS is much more triboelectrically negative than Al. When the Al foils starts to separate from PDMS film, electric potential difference (EPD) occurs. The EPD will drive electrons from electrode layer to Al foil, which results in the observed current flow i as shown in Fig. 2(ii). Due to the inflow of negative charges, positive charges on Al foil will be gradually neutralized until the PVDF cantilever vibrates down to impact with the lower outer frame as shown in Fig. 2(iii). After that, the Al foil separates from the lower PDMS film due to the periodic vibration. Electrons will flow back from Al foil to electrode because of electrostatic induction and positive charges are gathered on Al surface again as shown in Fig. 2(iv). At last, the two contact surfaces impact with each other as the initial state. Therefore, AC current can be generated from the upper triboelectric part of the hybrid WEH device. There is a similar charge transfer process of the lower triboelectric part. The current waveform is similar as the upper part but with a phase difference of a half cycle.

The characterization of the hybrid WEH device is conducted by using an air flow testing system, which consists of a mini wind tunnel (WTM-1000, Omega Company), an anemometer (HHF11A), and an oscilloscope. Fig. 3(a) and (c) show the open circuit peak voltages of the piezoelectric and upper triboelectric parts as wind speed increases from 2 to 14 m/s. The cut-in wind speed of the hybrid WEH device is 4 m/s. As the wind flow reaches 4 m/s, the PVDF cantilever is driven to vibrate gradually and the contact surfaces of the triboelectric part start to impact with each other. The open circuit peak voltages of the piezoelectric and upper triboelectric part are 5.6 and 3.8 V, respectively. With the increase of wind speed, larger deformation of the PVDF cantilever is achieved and the impact of Al-PDMS surface pairs becomes stronger. Therefore, the open circuit peak voltages of both parts increase gradually. There is an approximate linear correlation between peak voltage output and wind speed. At a wind speed of 14 m/s, the open circuit peak voltages of the piezoelectric and upper triboelectric parts are 19.8 and 17.4 V, respectively. Fig. 3(b) and (d) show the voltage waveforms of these two parts at wind speed of 10 m/s. The open circuit peak voltages are 16 and 13.4 V, respectively, at an oscillating frequency of 13 Hz.

The load characteristics of the hybrid WEH device are measured at varied wind speeds. Load resistances varying from 0.1 to 100 MΩ are used to obtain the corresponding averaged peak voltages and the power outputs can be calculated by U_{load}^2/R_{load}. As shown in Fig. 4(a), the instantaneous power output of piezoelectric part reaches a maximum value of 112 μW at an optimized load resistance of 0.6 MΩ and wind speed of 10 m/s. The output power of the upper

TABLE I
SUMMARY OF REPORTED PIEZOELECTRIC AND TRIBOELECTRIC WEHS

Reference	Transduction mechanism	Size (mm^3)	Wind speed (m/s)	Maximum Power (μW)	Power Density ($\mu W/cm^3$)
Liu [11]	Piezoelectric	3.3 × 2 × 0.4	15.6	0.0387	14.7
He [12]	Piezoelectric	3.7 × 7.4 × 0.51	11.7	2.4	172
Kwon [20]	Piezoelectric	100 × 60 × 30	4	4000	22.2
Bryant [21]	Piezoelectric	254 × 25.4 × 0.38	7.9	2200	748
This work	**Piezoelectric**	**52 × 16 × 0. 21**	**10**	**112**	**641**
Xie [7]	Triboelectric	Φ150 ×100	18	5100	6.7
Meng [10]	Triboelectric	90 × 50 × 3	10	107	7.93
Seol [22]	Triboelectric	40 × 31 × 3.2	3	0.9	0.24
This work	**Triboelectric**	**105 ×16 ×10**	**10**	**144**	**8.57**

triboelectric part can be obtained as 76 μW at 0.9 MΩ. The lower triboelectric part can also achieve an instantaneous power of 68 μW. Fig. 4(b) shows the output power at wind speeds of 4 to 14 m/s.

To further evaluate the output performance, the hybrid WEH device is compared with several reported piezoelectric and triboelectric WEHs as listed in Table I. It can be seen that our device shows excellent performance in terms of power density at a relatively low wind speed.

III. CONCLUSION

In conclusion, a hybrid flapping-blade WEH was proposed, which has advantages of ingenious structure, low-cost and high output. Both the piezoelectric and triboelectric parts can generate power from periodic vibration of the PVDF cantilever induced by vortex shedding effect. A flapping-blade is used to amplify the vibration of PVDF cantilever and enhance the contact force of Al-PDMS. Besides, outer frames are designed as spindle-shape to improve the power output of the triboelectric part. The maximum power of the piezoelectric and upper triboelectric parts can be obtained as 112 and 76 μW, respectively, at a wind speed of 10 m/s.

REFERENCES

[1] M. Kenisarin and K. Mahkamov, "Solar energy storage using phase change materials," *Renew. Sustain. Energy Rev.*, vol. 11, no. 9, pp. 1913–1965, 2007.

[2] Y. Hu, J. Yang, Q. Jing, S. Niu, W. Wu, and Z. L. Wang, "Triboelectric nanogenerator built on suspended 3D spiral structure as vibration and positioning sensor and wave energy harvester," *Acs Nano*, vol. 7, no. 11, pp. 10424–10432, 2013.

[3] C. Zhang, X.-F. He, S.-Y. Li, Y.-Q. Chen, and Y. Rao, "A wind energy powered wireless temperature sensor node," *Sensors*, vol. 15, no. 3, pp. 5020–5031, 2015.

[4] J. Xie, C. Lee, and H. Feng, "Design, fabrication, and characterization of CMOS MEMS-based thermoelectric power generators," *J. Microelectromech. Syst.*, vol. 19, no. 2, pp. 317–324, Apr. 2010.

[5] H. Liu, Z. Ji, T. Chen, L. Sun, S. C. Menon, and C. Lee, "An intermittent self-powered energy harvesting system from low-frequency hand shaking," *IEEE Sensors J.*, vol. 15, no. 9, pp. 4782–4790, Sep. 2015.

[6] S. Priya, "Modeling of electric energy harvesting using piezoelectric windmill," *Appl. Phys. Lett.*, vol. 87, no. 18, p. 184101, Oct. 2005.

[7] Y. Xie *et al.*, "Rotary triboelectric nanogenerator based on a hybridized mechanism for harvesting wind energy," *Acs Nano*, vol. 7, no. 8, pp. 7119–7125, 2013.

[8] C. Sun *et al.*, "A miniaturization strategy for harvesting vibration energy utilizing Helmholtz resonance and vortex shedding effect," *IEEE Electron Device Lett.*, vol. 35, no. 2, pp. 271–273, Feb. 2014.

[9] S. Wang, X. Mu, Y. Yang, C. Sun, A. Y. Gu, and Z. L. Wang, "Flow-driven triboelectric generator for directly powering a wireless sensor node," *Adv. Mater.*, vol. 27, no. 2, pp. 240–248, 2015.

[10] X. S. Meng, G. Zhu, and Z. L. Wang, "Robust thin-film generator based on segmented contact-electrification for harvesting wind energy," *ACS Appl. Mater. Interfaces*, vol. 6, no. 11, pp. 8011–8016, 2014.

[11] H. Liu, S. Zhang, T. Kobayashi, T. Chen, and C. Lee, "Flow sensing and energy harvesting characteristics of a wind-driven piezoelectric $Pb(Zr_{0.52}, Ti_{0.48})O_3$ microcantilever," *IET Micro Nano Lett.*, vol. 9, no. 4, pp. 286–289, 2014.

[12] X.-F. He and J. Gao, "Wind energy harvesting based on flow-induced-vibration and impact," *Microelectron. Eng.*, vol. 111, no. 11, pp. 82–86, 2013.

[13] X. Wang, C. L. Pan, Y. B. Liu, and Z. H. Feng, "Electromagnetic resonant cavity wind energy harvester with optimized Reed design and effective magnetic loop," *Sens. Actuators A, Phys.*, vol. 205, no. 1, pp. 63–71, 2014.

[14] S. Li, J. Yuan, and H. Lipson, "Ambient wind energy harvesting using cross-flow fluttering," *J. Appl. Phys.*, vol. 109, no. 2, p. 026104, 2011.

[15] J. M. McCarthy, A. Deivasigamani, S. J. John, S. Watkins, F. Coman, and P. Petersen, "Downstream flow structures of a fluttering piezoelectric energy harvester," *Experim. Thermal Fluid Sci.*, vol. 51, no. 11, pp. 279–290, 2013.

[16] L. Dhakar, F. E. H. Tay, and C. Lee, "Investigation of contact electrification based broadband energy harvesting mechanism using elastic PDMS microstructures," *J. Micromech. Microeng.*, vol. 24, no. 10, p. 104002, 2014.

[17] M. Han *et al.*, "r-shaped hybrid nanogenerator with enhanced piezoelectricity," *Acs Nano*, vol. 7, no. 10, pp. 8554–8560, 2013.

[18] Y. Zhu, B. Yang, J. Liu, X. Wang, X. Chen, and C. Yang, "An integrated flexible harvester coupled triboelectric and piezoelectric mechanisms using PDMS/MWCNT and PVDF," *J. Microelectromech. Syst.*, vol. 24, no. 3, pp. 513–515, Jun. 2015.

[19] X.-S. Zhang, M.-D. Han, B. Meng, and H.-X. Zhang, "High performance triboelectric nanogenerators based on large-scale mass-fabrication technologies," *Nano Energy*, vol. 11, pp. 304–322, Jan. 2015.

[20] S.-D. Kwon, "A T-shaped piezoelectric cantilever for fluid energy harvesting," *Appl. Phys. Lett.*, vol. 97, no. 16, p. 164102, 2010.

[21] M. Bryant and E. Garcia, "Modeling and testing of a novel aeroelastic flutter energy harvester," *J. Vib. Acoust.*, vol. 133, no. 1, pp. 253–256, 2011.

[22] M.-L. Seol *et al.*, "Vertically stacked thin triboelectric nanogenerator for wind energy harvesting," *Nano Energy*, vol. 14, pp. 201–208, May 2015.